

**Relationship between precipitation in the Great Plains of the United States and
global SSTs: Insights from the IPCC-AR4 models**

Antonietta Capotondi
NOAA Earth System Research Laboratory, and University of Colorado/CIRES

Michael A. Alexander
NOAA Earth System Research Laboratory

Corresponding author address:

Antonietta Capotondi, NOAA/ESRL/PSD, 325 Broadway, Boulder, CO, 80305

Email: Antonietta.Capotondi@noaa.gov

Phone: 303-497-6105

Fax: 303-497-6449

Abstract

Multi-century pre-industrial control simulations from six of the IPCC-AR4 models are used to examine the relationship between low-frequency precipitation variations in the Great Plains (GP) region of the United States (U.S.) and global sea surface temperatures (SSTs). This study builds on previous work performed with atmospheric models forced by observed SSTs during the 20th century, and extends it to a coupled model context, and longer time series. The climate models used in this study reproduce the precipitation climatology over the U. S. reasonably well, with maximum precipitation occurring in early summer, as observed. The modeled precipitation time series exhibit negative “decadal” precipitation anomalies, identified using a 5-year running mean, of amplitude comparable to that of the 20th century droughts. It is found that low-frequency precipitation anomalies over the GP are part of a large-scale pattern of precipitation variations, characterized by anomalies of the same sign as in the GP region over Europe and southern South America, and anomalies of opposite sign over northern South America, India, and Australia. The large-scale pattern of the precipitation anomalies is associated with global-scale atmospheric circulation changes: during wet periods in the GP, geopotential heights are raised in the Tropics and high-latitudes and lowered in the mid-latitudes in most models, with the mid-latitude jets displaced toward the equator in both hemispheres. Statistically significant correlations are found between the decadal precipitation anomalies in the GP region and tropical Pacific SSTs in all the models. The influence of other oceans (Indian, tropical and North Atlantic), which previous studies have identified as potentially important, appears to be model dependent.

1. Introduction

The western United States, including the Great Plains, is particularly vulnerable to multi-year droughts. Recent examples during the 20th century are the decade-long drought of the 1930s, which mainly affected the Great Plains area, the dry period from the late 1940s to the late 1950s in several regions of the southwest, as well as the several years of reduced precipitation after the demise of the 1997/1998 El Niño. During the 1930s, the degree of aridity in the Great Plains area was so severe that all drought-sensitive crops died, and dust storms devastated the area, which became known as the “Dust Bowl”. Long-term droughts in the American West were not limited to the 20th century. Paleoclimate evidence (Stine 1994, Cook et al. 2004, Herweijer et al. 2007) indicate that a series of severe droughts occurred in the western United States starting at ~600 AD, and continuing into the 14th century, the most probable cause of the abandonment of the ancestral Pueblo Indians sites at the beginning of the 15th century (Douglass 1929, 1935, Dillehay 1974, Jones et al. 1999, Benson et al. 2007). This time coincided with the Medieval Warm Period in Europe (800 AD to 1400 AD), indicating that long-lasting droughts in the western U.S. may be associated with global scale precipitation anomalies (Seager et al. 2007). In particular, dry conditions in western North America tend to be associated with dry conditions across the mid-latitude North Atlantic Ocean, the Mediterranean, including parts of Europe and the Middle East, as well as central Asia (Hoerling and Kumar 2003). Sparse paleoclimate evidence also indicates that when North America is dry, it is wet in northern South America, dry in southern South America, southern Europe and the Mediterranean, and in equatorial East Africa, wet in the Sahel, South Africa, as well as India (Seager et al. 2007).

Numerical simulations performed with atmospheric models driven by observed sea surface temperatures (SSTs) indicate that the major droughts in the 20th century are partly driven by subtle changes in tropical SSTs (Schubert et al. 2004a,b; Seager et al. 2005). Schubert et al. (2004a, b) were able to reproduce the “Dust Bowl” drought as the ensemble average of their SST-forced atmospheric simulations, although there was considerable scatter among the different ensemble members, an indication of the important influence of internal atmospheric variability upon the evolution of precipitation

over North America. Sensitivity experiments, where SST anomalies were prescribed only in selected regions showed the key role of tropical Pacific SSTs, although the tropical Atlantic can also have a significant contribution in driving precipitation variations over North America. The largest influences upon dry conditions in the western U. S. are found when the tropical Pacific is anomalously cold, like during La Niña events, and the tropical Atlantic is warmer than average (Schubert et al. 2004a). Warm conditions in the western tropical Pacific and Indian Ocean can also contribute to dry conditions over the United States (Hoerling and Kumar 2003), as found during the 1998-2002 drought.

More recently, Seager et al. (2008) have shown that ensemble simulations driven by observed SSTs over the 1930s period produced a drought signal over the U.S. which significantly differed from the model climatology, while the precipitation signal obtained with climatological SST forcing was not statistically distinguishable from the model climatology, supporting the idea that SST forcing can play a significant role in the occurrence of droughts over the central U. S., and can increase prediction capabilities. Significant correlations between summer precipitation and Pacific SSTs were also noted by Ting and Wang (1999) at interannual timescales.

The SST-forced atmospheric simulations of Schubert et al. (2004a, b) and Seager et al. (2005, 2008) showed that precipitation anomalies in the western U. S. were part of a global-scale pattern of precipitation changes, consistent with the paleoclimate evidence. The global-scale character of those changes appears to be related to the global-scale atmospheric circulation anomalies, a response to anomalous SSTs similar to that found during El Niño Southern Oscillation (ENSO) events (Seager et al. 2005). During warm tropical conditions, tropical upper-troposphere geopotential heights are raised, consistent with tropical warming, while heights are lower in the midlatitudes.

The mechanism by which tropical Pacific SST anomalies influence precipitation in the American West involves changes in strength and position of the subtropical jets in both hemispheres, changes in transient eddies and eddy-induced meridional flow (Seager et al. 2005). When the tropical Pacific is cold, the equator-to-pole tropospheric temperature gradient decreases, and the subtropical jet streams weaken and move poleward. The resulting atmospheric adjustment involves an eddy-induced poleward flow, creating areas of mass convergence, where descending motion, responsible for

suppressing precipitation, must take place. Changes in tropical Pacific SSTs can also alter the mean atmospheric circulation through changes in the location of the major tropical heating sources.

Meehl and Hu (2006) have examined the relationship between long periods of precipitation deficit in the southwestern North America and global SSTs in a 1360-yr-long control integration of the Parallel Climate Model (PCM), a fully coupled climate model. The focus of this study was on “megadroughts”, defined as 11-yr running mean regional area-averaged negative precipitation anomalies lasting for at least 20 years. A statistically significant correlation was found between the low-frequency evolution of precipitation in the southwestern North America and low-frequency Pacific SST anomalies. The correlation pattern is very similar to the leading mode of Pacific decadal SST variability in the model, which is, in turn, in very good agreement with the spatial pattern of the Interdecadal Pacific Oscillation (IPO) as described by Power et al. (1999) and Arblaster et al. (2002). This pattern is characterized by anomalies of the same sign in a broad triangular-shaped region centered along the equatorial Pacific, and anomalies of opposite sign in the central-western mid-latitudes of both hemispheres, and is similar to the Pacific Decadal Oscillation (PDO) computed by Mantua et al. (1997) over the North Pacific.

In this study we examine the connection between multi-year precipitation anomalies in the western U.S. and global SSTs in a subset of the climate models developed in support of the Intergovernmental Panel for Climate Change (IPCC) Assessment Report 4 (AR4). In particular, we are interested in examining whether, and to what extent, the results obtained with ensembles of Atmospheric Model Inter-comparison Project (AMIP)-type simulations performed with the same model (e.g. Schubert et al. 2004a, and Seager et al. 2005) are found across a suite of fully-coupled climate models. The IPCC models differ in both spatial resolution and physical parameterizations in each of their component models, but have been run in similar configurations, and with similar anthropogenic forcing. For this study we will focus on the pre-industrial control integrations (PICNTRL) whose multi-century duration allows a better characterization of multi-year droughts. In addition, since the greenhouse gas concentration is kept fixed at the pre-industrial level in the PICNTRL simulations, the relationship between SST and

precipitation can be examined in the context of natural climate variability. The specific questions that we ask are: 1) Is the SST-precipitation relationship in the climate models consistent with what has emerged from observations and AMIP simulations?; 2) Is the large-scale signature of drought conditions in the central U.S. from the IPCC-AR4 models in agreement with the evidence from paleoclimate and proxy records, like those described by Seager et al. (2007)?, and 3) Are the SST anomalies associated with central U.S. droughts related to the dominant mode of Pacific SST variability in the different models? Following Schubert et al. (2004a, b), we will focus on the evolution of precipitation in the region of the Great Plains (GP).

The paper is organized as follows: in section 2 we describe the models used for this study, as well as the observational data sets used to validate the models; in section 3 we examine the model representation of mean precipitation over North America to assess how reliable the models are; in section 4 the evolution of precipitation over the Great Plains region is considered, as well as the associated global patterns of precipitation, SST, and atmospheric circulation anomalies. The relationship between the precipitation changes and the leading mode of Pacific SST variations is examined in section 6, and conclusions are provided in section 7.

2. Models and data

We examine the pre-industrial control simulations (PICNTRL) from six of the IPCC climate models, as listed in Table 1. The pre-industrial control simulations are multi-century simulations with the chemical composition of the atmosphere fixed at pre-industrial conditions. The absence of any anthropogenic forcing in these simulations allows us to focus on natural variability only. The model outputs have been collected at the Program for Climate Model Diagnosis and Intercomparison (PCMDI). The models have been chosen based on the availability of their ocean data, as well as the duration of their pre-industrial control integrations, which we wanted to be at least 300 yrs, to better characterize low-frequency precipitation evolution and decadal climate variability. The duration of the PICNTRL simulation for each model is shown in the last column of Table 1. As seen from the second and third column of Table 1, the models differ considerably in

both horizontal and vertical resolutions. The numerical grids used by each model are also different. For example, the ocean component of CCSM3 is based on the Parallel Ocean Program (POP), and uses a bipolar grid with the northern pole displaced over Greenland. Most ocean components have finer meridional grid spacing in the Tropics, to resolve the jet-like structure of the equatorial circulation. Physical parameterizations of sub-grid scale processes, such as convection and mixing also differ among models.

Due to the coarse horizontal resolution of the atmospheric components of the climate models, the representation of precipitation over North America may be unrealistic. To validate the model precipitation fields we use the precipitation climatology developed at the Global Precipitation Climatology Center (GPCC, <http://gpcc.dwd.de>). This data set uses a large number of rain gauge based precipitation data to produce a monthly climatology interpolated on a $1^\circ \times 1^\circ$ grid from 1901 to 2007. SSTs data from the Extended Reconstructed data set developed at the National Atmospheric and Oceanic Administration (NOAA.ERSST, Reynolds et al. 2008), also available as monthly means on a $1^\circ \times 1^\circ$ grid from 1854 through present has been used to provide an observational term of comparison for the precipitation-SST relationship, as well as for the patterns of the leading modes of SST variability. Since SST observations in the 1800s are sparse, and the quality of the reconstructed data may be somewhat questionable, only values after 1900 have been used.

3. Mean precipitation over North America

The annual mean precipitation from the GPCC data set (Figure 1) is characterized by precipitation maxima along the coastal regions of the American Northwest, and in the area close to the Gulf of Mexico, with decreasing values in the central and southwestern areas of the United States. Following Schubert et al. (2004a), we will focus on the region of the Great Plains (95° - 105° W, 30° - 50° N), as shown by the box in Figure 1. The GP lie in the region of large zonal gradients of mean precipitation, and can be affected by variations in the moisture supply from the Gulf of Mexico.

The mean precipitation in the models, computed as the annual average over the total duration of the PICNTRL simulations (Figure 2) also shows maxima in both Northwest

and Southeast of the United States, but the spatial extension, amplitude, as well as exact locations of the maxima are not represented correctly. For example, the precipitation maximum near the Gulf of Mexico is displaced north of Florida in all the models, and the precipitation gradients across the GP are not zonal and tend to be more diffuse in the models compared to observations. Overall, the models tend to slightly underestimate precipitation in the southeastern U.S., and overestimate precipitation in the central and southwestern United States. These results are consistent with the findings of McAfee and Russell (2009), who have examined wind speeds and cold season (November-April) precipitation in the 20th century simulations of eighteen models from the IPCC-AR4 archive. They found that the model's attenuation of orography over the Rocky Mountains is responsible for increasing the zonality of the atmospheric circulation, leading to higher wind speeds around 30°N, and to wet biases over western North America, as well as to a general distortion of the precipitation pattern.

The seasonal evolution of precipitation is also very important. Over the GP the observed precipitation evolution (black line in Figure 3) achieves maximum values of ~2.5 mm/day in May-June, with a slow decrease during the late summer/fall months to minimum winter values of ~0.6 mm/day. The values in Figure 3 are based on the area-averaged precipitation over the Great Plains box in Figure 1. The models show a qualitatively similar seasonal evolution, with maxima in late spring/summer. Some models (GFDL_CM2.0, GFDL_CM2.1, and UKMO_HadCM3) have overall larger values, as indicated by the annual averages (numbers in parenthesis), while other models (CCSM3, CSIRO, CCCMA) have annual averages of precipitation very close to the observed, but the seasonal evolution decreases too rapidly in late summer/early fall. The GFDL_CM2.1 and the GFDL_CM2.0 have a seasonal evolution of precipitation throughout the year similar to that from GPCC, but with much larger values, especially at the peak (~4.3 mm/day for GFDL_CM2.1, and 4.1 mm/day for GFDL_CM2.0). The amplitude of the seasonal cycle in the models GP region is largely related to the position of the GP area, as identified by the boxes in Figure 2, relative to the spatial pattern of the models wet biases, as well as the magnitude of the biases. As seen in Figure 2, the GP region significantly overlaps areas of larger than observed precipitation in GFDL_CM2.1, GFDL_CM2.0, and UKMO_HadCM3. Similar biases are found in the seasonal evolution

of precipitation in the core region of the North America monsoons (central-northwest Mexico, and a small portion of Texas), as diagnosed in the 20th century simulations of the IPCC-AR4 models by Liang et al. (2008). The representation of interannual monsoon variability, likely associated with larger-scale processes, was more realistic in the models. In spite of the models deficiencies in the representation of GP precipitation, we think that they can be useful for examining the relationship between precipitation and SST.

4. Low-frequency precipitation evolution in the Great Plains region

The observed evolution of precipitation over the 20th century, and beginning of the 21st century, as rendered by the GPCC data set, is shown in Figure 4a. The thin curve in Figure 4 is for annual precipitation anomalies, while the thick curve is obtained by applying a 5-yr running mean to the annual values, in order to isolate “decadal” droughts. Multi-year periods of precipitation deficits can be seen around 1910, as well as in the 1930s and 1950s. Low-pass filtered precipitation anomalies during the 1930s and 1950s droughts are of the order of 0.2 mm/day, which is approximately 13% of the annual mean precipitation (1.57 mm/day, Figure 3). The standard deviation of the low-pass filtered time series is 0.11 mm/day.

While Figure 4a provides an annually-averaged perspective of the precipitation evolution, it is also important to determine the seasonal dependency of the precipitation anomalies. Figure 4b shows the standard deviation of the decadal precipitation anomalies as a function of calendar month. A 5-yr running mean has been applied to the time series for each individual month, prior to computing the standard deviation shown in Figure 4b. The largest anomalies are found in summer (June-July), the rainy season, with a second maximum in October. While the large June-July standard deviation is somewhat expected, the large October standard deviation is more intriguing, and we do not have an explanation for the October large precipitation variations. The maxima in July and October differ from the August minimum with a large statistical confidence, based on an F-test.

The low-pass filtered (5-yr running mean applied to annually averaged values) evolution of precipitation over the Great Plains region in the six IPCC models (Figure 5)

also shows the occurrence of multi-year periods of precipitation deficit. To compare the model simulated droughts with the major droughts of the 20th century, we will use a loose definition of “decadal droughts”, as periods with lower-than-average precipitation lasting for more than ~5 years in the 5-year running mean time series. The standard deviation of the time series (shown in the bottom-right corner of each panel) is similar to that of the observed time series, and the magnitude of some of the negative precipitation anomalies, relative to the mean annual precipitation, is also comparable to that associated with the 20th century droughts. For example, for the GFDL_CM2.1 low-frequency precipitation anomalies are as large as 0.3 mm/day, which is about 14% of the mean annual value (2.13mm/day, Figure 3), a value comparable to the 13% obtained for the observational time series. The seasonal distribution of the decadal precipitation anomalies in the models, as described by monthly standard deviations is shown in Figure 6. Except for CCSM3, the models have two standard deviation maxima, one in the summer and one in the fall, as in the observations, but either the maxima are not as large as in the observations or the late summer decrease in standard deviation is not as pronounced. CCSM3 shows a large maximum in July, but the standard deviations decrease rapidly in late summer and remain low throughout the fall and winter.

To examine whether precipitation anomalies in the GP region are associated with large-scale SST and precipitation changes, as found in AMIP simulations, we start by computing composites of the SST and precipitation conditions during periods of extensive precipitation deficit in the GP. An example from the GFDL_CM2.1 is given in Figure 7, which shows average SST (blue-red shading over the ocean) and precipitation over land (brown-green shading over land) anomalies during years 38-55, 170-175, and 240-255, periods highlighted by the red lines in Figure 5. In all three periods chosen, there are cold conditions in some areas of the tropical Pacific, as well as in the eastern North and South Pacific, with anomalies of opposite sign in the western midlatitudes. Anomalies in other oceans are less consistent from period to period. For example, the North Atlantic is cold in years 38-55, but has some warm areas in the other two periods. The average composite (bottom-right panel) shows that the large SST anomalies are found in the Pacific. In the tropical Pacific the coldest conditions are located in the western half of the basin, with maximum values of ~0.5°C. The differences in the SST

pattern seen in the three composites are consistent with the differences in the average SST conditions during observed droughts (see Figure 3 in Seager et al. 2007, showing the SST patterns for the periods 1890-1896, 1932-1939, and 1948-1957, all characterized by lower-than-average precipitation in the central U.S.)

When the GP are dry, all the composites and their average show that dry conditions also occur over Europe, some parts of Asia, central Africa, and southern South America, while northern South America, southern Africa, India, and Australia are anomalously wet, consistent with paleoclimate evidence (Seager et al. 2007).

Did the precipitation remained below average during the whole duration of the three drought periods considered for the GFDL_CM2.1, and are the cold conditions in the western tropical Pacific during all three periods an indication that the SSTs in the western side of the basin play a more important role than those in the eastern side of the basin? Figure 8 shows the evolution of GP precipitation in the GFDL_CM2.1 model over the first hundred years of the PICNTRL simulation, and during the 160-260 time period, based on annual values. The low-pass filtered curve (thick curve, same as in Figure 5a) is also shown for comparison. Although, on average, the precipitation was below normal during the three composite periods considered in Figure 7, there were large year-to-year excursions in all three periods. Between years 38 and 55 there were two years when the precipitation was back to average conditions, and between year 240 and 254 there were two years in which the precipitation was above normal. To clarify the relationship between the evolution of precipitation and SST in both sides of the equatorial Pacific we consider two equatorial boxes: a western Pacific box, 140°E-180°E, 5°S-5°N, and an eastern Pacific box, 150°W-110°W, 5°S-5°N. The SST evolution in the western box for the two century-long periods considered is shown in Figures 8c and d, respectively, while the SST evolution in the eastern box is shown in the lower panels of Figure 8. In the western equatorial Pacific the SST anomalies tend to be biased toward negative values. Positive anomalies are not warmer than 1°C, while negative anomalies can be as large as -2.5°C. During the periods considered for the composites (highlighted with a thicker line in Figures 8c-f) the western equatorial Pacific was colder than average. In the eastern equatorial Pacific, on the other hand, SSTs underwent large positive and negative interannual variations, resulting in average conditions, over decadal periods, which are

closer to neutral. During years 38-55, and 240-254 the positive anomalies in the eastern Pacific coincide with the return to normal or above-average conditions in GP precipitation (thin line in top panels of Figure 8). Thus, the eastern Pacific appears to be important for the evolution of precipitation over the GP region in this particular model, but its influence seems stronger at interannual timescales. This is most likely due to the greater interannual SST variability rather than to a change in the teleconnections as a function of frequency.

Another approach to examine the relationship between GP precipitation and global SSTs and precipitation is through correlation analysis. We start by considering the correlation between the observed precipitation time series and SST from the NOAA.ERSST dataset. All time series have been low-passed filtered by applying the 5-year running mean. Figure 9 shows the correlation pattern over the Global Ocean. Large positive correlations (positive SST anomalies are associated with positive precipitation anomalies in the GP region) are found in a triangular region centered along the equatorial Pacific and extending toward the midlatitudes along the western coast of the Americas. Positive correlations are also found in the South Pacific, South Atlantic and Indian Ocean, while large negative correlations are present in the North Atlantic. The number of degrees of freedom, computed following Trenberth (1984), varies geographically from 10 to 20 degrees of freedom in the central and eastern equatorial Pacific. Thus only correlations larger than ~ 0.45 in the tropical and South Pacific, as well as North Atlantic are statistically significant at the 95% level, based on a t-test approach.

A similar correlation analysis is performed for the six climate models (Figure 10). Due to the multi-century duration of the models output, the number of degrees of freedom is larger than for observations, exceeding 80 for the two GFDL models and CCSM3, and 60 for HadCM3, CSIRO, and CCCMA over a large part of the ocean. Correlations larger than ~ 0.2 are statistically significant at the 95% level for the first three models, while for HadCM3, CSIRO, and CCCMA statistically significant correlations must be larger than ~ 0.25 . Results from the models confirm the central role of the tropical Pacific, where statistically significant positive correlations are found in all the models. Although the exact locations of maximum correlations vary among models, in all cases the spatial pattern of correlation in the Pacific has a triangular structure

similar to that seen in Figure 9 for observations. GFDL_CM2.1, HadCM3, and CSIRO have statistically significant positive correlations in the Indian Ocean, and tropical Atlantic. Significant correlations in the South Pacific are only found for GFDL_CM2.1, and CSIRO. Except for CCSM3 and GFDL2.0, the correlation patterns in Figure 10 are similar to the patterns of the leading SST Empirical Orthogonal Functions (EOFs), which are shown in Figure 15, and discussed later in section 5, an indication that midlatitude SST anomalies in those models are correlated with the tropical SST anomalies. Thus, the presence of statistically significant correlations in the extra-tropics does not necessarily imply that those anomalies directly force GP precipitation. Indeed, as shown in sensitivity studies using AMIP-type simulations where anomalous SSTs were specified only in selected regions (Schubert et al. 2004a, Seager et al. 2005) only tropical SST anomalies were relevant in forcing GP precipitation.

The correlations between low-frequency precipitation in the Great Plains and the global precipitation field are shown in Figure 11. Values larger than ~ 0.2 are statistically significant at the 95% level. Although the precipitation patterns are noisier than the SST correlation patterns, the global character of the precipitation changes clearly emerges in Figure 11, with characteristics similar to those described by Schubert et al. (2004a). Wet conditions in the Great Plains are associated with increased precipitation in the western equatorial Pacific, and along a band extending southeastward from the western tropical Pacific to the tip of South America. Positive precipitation anomalies are found over Europe and/or the Mediterranean area in most models, but they tend to be below the 95% significance level. Negative correlations (dry conditions) are found over India and Australia, as well as Central and northern South America. Notice that there are large differences among models in the magnitude of the correlations away from the GP region. In particular, CCSM3 and, to a lesser degree, CCCMA have very weak correlations. In CCSM3, the only statistically significant correlations (greater than 0.2) are in the western equatorial Pacific, and in a small area offshore of the western coast of southern South America.

The changes in precipitation over the globe forced by SST anomalies can be expected to occur through atmospheric teleconnections. Figure 12 shows the correlation between low-frequency precipitation in the GP and low-frequency 200 mb geopotential height.

The geopotential height anomalies are characterized by a banded structure with a high degree of zonal symmetry, similar to those described in the AMIP studies of Schubert et al (2004a), and Seager et al. (2005). Wet conditions over the GP region are associated with raised heights in the Tropics and in high-latitudes, but lower heights in the mid-latitudes. One exception is CCSM3, where lower heights are also found in the northern high-latitudes. The models consistently show localized lows close to the western coast of the U.S., displaced westward with respect to the GP region, and in the central North Pacific, which may be associated to increased storminess, as pointed out by Schubert et al. (2004a). Although the general structure is similar in most of the models, the intensity of the correlations vary significantly from model to model, ranging from maximum values of 0.2-0.3 in the CCSM3 and CCCMA to values as large as 0.6 in the CSIRO model, where positive correlations dominate. The low correlations in the CCSM3 and CCCMA models may be a consequence of a weak atmospheric response to SST anomalies, or result from the magnitude and/or location of the SST anomalies themselves. The weak atmospheric signal in these models may explain the more limited precipitation response seen in Figure 11.

Which changes in the atmospheric circulation are associated with the changes in geopotential height? The large degree of zonal symmetry in the height field justifies a zonal average perspective. Figure 13 shows correlations between decadal precipitation anomalies in the GP region and temporal anomalies in the zonal mean zonal wind. As for all other fields, anomalies have been computed by subtracting the long-term mean from the annually averaged values prior to applying the 5-year running mean. The correlations are displayed superimposed upon the mean zonally averaged positive wind velocities, showing the mean position of the midlatitude jets. Correlation larger than ~ 0.2 are statistically significant at the 95% level. With the exception of the CCSM3, all the models show negative correlations on the poleward flanks of the jets, and positive correlation on the equatorward sides of the jets, indicative of an equatorward displacement of the midlatitude jets during periods of larger than average GP precipitation, which, in turn, tend to be concurrent with warm conditions in the tropical Pacific. Correlations are particularly large in the GFDL_CM2.1, HadCM3, and CSIRO models. GFDL_CM2.1, HadCM3, and CCCMA show slightly larger correlations in the

northern hemisphere. The changes in atmospheric circulations implied by the correlation patterns in Figure 13 are in agreement with the results of Lu et al. (2008, their Figure 2c), who examined the changes in the zonal mean atmospheric circulation due to El Niño vs. global warming in the A2 (high-forcing) climate change scenario simulation of the 21st century performed with the GFDL_CM2.1 model. The changes in the zonal mean atmospheric circulation associated with natural interannual variability show a contraction (expansion) of the Hadley cell during El Niño (La Niña) events similar to those seen in Figure 13. Global warming, on the other hand, results in weakening and poleward expansion of the Hadley cell in spite of the tropical warming.

5. Relationship between Pacific SST anomalies and modes of SST variability

The pattern of correlations between GP precipitation and SST in the tropical Pacific is reminiscent of the structure of the IPO (Power et al. 1999), the Interdecadal Pacific Oscillation, as also discussed in previous studies (Schubert et al. 2004a, Meehl and Hu 2006). To elucidate the connection between low-frequency precipitation variations in the GP region, and the leading mode of low-frequency SST variations, we perform a EOF analysis of the 5-year running mean SST field. We limit the analysis to the Pacific basin, which is the one that more consistently shows correlations with the GP precipitation in all the models. Figure 14a shows the leading SST EOF for the NOAA.ERSST dataset, based on covariance. The pattern of the mode, which explains 30% of the low-frequency SST variance, is similar to the well-known structure of the IPO (Power et al. 1999), and PDO in the Northern Hemisphere (Mantua et al. 1997). The corresponding Principal Component (PC, Figure 14b) has a correlation of 0.56 with the low-pass filtered GP precipitation time series, which is statistically significant at the 95% level, and marginally significant at the 99% level. However, Figure 14b shows that large precipitation anomalies, like the “Dust Bowl” in the 1930s, are not associated with large SST PC1 anomalies, as SSTs were only weakly negative during the “Dust Bowl” period, as also shown by the averaged SSTs during the 1930s (Schubert et al. 2004b). We note that the observed evolution of SST could be influenced by global warming, unlike the SST fields

from the models PICNTRL simulations. No significant trend can be detected in the evolution of the PC in Figure 14b, indicating that the EOF is primarily associated with natural variability.

The leading EOFs for the six climate models (Figure 15) exhibit differences in their spatial patterns. While GFDL_CM2.1, HadCM3, CSIRO, and, to a lesser degree, CCCMA, have spatial patterns for their leading decadal SST EOF qualitatively similar to the IPO pattern, in GFDL_CM2.0 and CCSM3 the tropical loading is much weaker than in the other models and in the observations. In those models the main centers of actions are in the North Pacific, with a spatial pattern similar to that described by Kwon and Deser (2007) for the NCAR Community Climate Model version 2 (CCSM2), an earlier version of the NCAR climate model. Kwon and Deser (2007) have shown that the leading mode of winter SST anomalies in the North Pacific have a pattern similar to the PDO, and is characterized by significant spectral peaks in the decadal and inter-decadal range. The western center of action is located along the Kuroshio Extension, and originates from wind-forced meridional excursions of the Kuroshio Extension. The SST anomalies force, in turn, an atmospheric wind response, so that this mode of variability can be considered a coupled ocean-atmosphere mode. It is likely that the leading EOFs for CCSM3 and GFDL_CM2.0 originate from a similar coupled dynamics. The lack of connection of the PDO with the Tropics in CCSM3 was also noted by Alexander et al. (2006).

The percentage of explained variance ranges from 20% in the CSIRO model to 29% in the GFDL_CM2.1 model, in relatively good agreement, for most models, with what found for the observed SST. The evolution of the corresponding PCs is compared in Figure 16 with the evolution of GP precipitation in all the models. Correlation coefficients between the time series, as well as the correlations corresponding to the 95% significance level, are shown in each panel. Apart from GFDL_CM2.0, and CCSM3, whose correlations between GP precipitation and PC1 are only marginally significant, all the other models have statistically significant correlations between the leading SST mode in the Pacific and precipitation in the GP region. The agreement between the two time series is particularly evident, by visual inspection as well as correlation coefficient, for HadCM3 and CSIRO, where the evolution of precipitation seems to track that of SST

very closely. The low correlation coefficients for CCSM3 and GFDL2.0 may be a result of their very weak tropical loading. In fact, at least for CCSM3, the only significant correlations between GP precipitation and SST are found in the tropical Pacific (Figure 10). Also, as demonstrated by other studies (Schubert et al. 2004a, Seager et al. 2005) tropical SST anomalies are the primary players in forcing U.S. precipitation. However, while the second SST EOF for CCSM3 (not shown) has a larger tropical loading, the correlation coefficient between PC2 and GP precipitation remains only marginally significant. The largest correlations in Figure 10 for CCSM3 are ~ 0.3 , implying that at the most only about 9% of the GP precipitation variations can be related to remote SST forcing. Thus, in this model low-frequency GP precipitation variations may be more locally driven. Given the low correlations between GP precipitation and atmospheric fields in CCSM3 at the global scale (Figures 12c and 13c) the primary cause of the weak SST influence on precipitation in this model may be associated with weak atmospheric teleconnections at decadal timescales, a factor that may limit the model predictive skills.

6. Conclusions

In this study we have examined the relationship between low-frequency precipitation in the Great Plains region of North America and sea surface temperature (SST) in six of the IPCC-AR4 climate models. This study builds upon, and extends to a coupled model context, previous studies performed with atmospheric-only models forced by observed SSTs. We have focused upon pre-industrial control simulations, whose multi-century duration allows us to examine the influence of low-frequency SST variations due to natural variability on U.S. precipitation with a large statistical confidence.

In spite of their coarse horizontal resolution, the IPCC climate models reproduce the general features of the spatial pattern of observed mean precipitation over North America, including maxima in the American Northwest, and Southeast, with lower values in the central United States. However, the large zonal gradients found in observations in the central U.S., are not as pronounced in the models, and the location of maximum precipitation in the Southeast is displaced with respect to the observed in most models. In the Great Plains region, the rainy season occurs in early summer, with precipitation

slowly decreasing toward the minimum winter values. All the models analyzed capture the early summer maximum, but in some of them the maximum, as well as the annual average values are too large. In other models, the summer values have approximately the correct amplitude, but the level of precipitation decreases too rapidly than observed in late summer and fall.

The evolution of low-pass filtered precipitation (using a 5-year running mean) exhibits multi-year periods of lower-than-average precipitation of amplitude comparable to that observed during the 19th century and early 20th century. Correlation analysis shows that long periods of anomalous precipitation in the Great Plains area are part of a global pattern of anomalous precipitation conditions. In particular, dry conditions in the Great Plains are concurrent with dry conditions over some parts of Europe, and southern South America, and wet conditions over northern South America, India, and Australia, in agreement with previous studies.

The large-scale pattern of precipitation anomalies is consistent with the large-scale pattern of atmospheric circulation anomalies. Wet conditions in the Great Plains are associated with raised geopotential heights in the Tropics and high-latitudes in most models, and lower heights in the mid-latitudes, with a structure characterized by a high-degree of zonal symmetry. When the Great Plains are wet, the midlatitude jets tend to be displaced equatorward. These changes in atmospheric circulation are consistent with those accompanying a warm tropical Pacific, as during El Niño events (Seager et al. 2005, Lu et al. 2008).

Correlation analysis between Great Plains low-frequency precipitation and low-frequency SST anomalies shows indeed statistically significant correlations between precipitation and SST in the tropical Pacific. The pattern of correlation has a triangular-shaped pattern with positive values extending toward the mid-latitudes along the western coast of the Americas. In some models negative correlations are found in the central-western mid-latitudes of the Pacific, and statistically significant positive correlations are found, in some cases, in the tropical Atlantic and Indian Ocean. However, the tropical Pacific is the only area that consistently emerges, among the models analyzed, as statistically significant correlated with Great Plains precipitation.

The spatial pattern of correlation between the observed Great Plains precipitation and SST is somewhat similar to the leading mode of Pacific SST variability at decadal timescales, named the Interdecadal Pacific Oscillation by Power et al. (1999). The associated principal component tracks relatively well the low-frequency evolution of precipitation over the Great Plains region. A similar correspondence is found for most of the models, but in some cases the correlation between principal component and precipitation is very marginally significant. In these models, the leading SST EOF has a weak loading in the tropical Pacific, with the major centers of action located in the North Pacific, further supporting the evidence that the tropical Pacific is a key area for driving atmospheric circulation and precipitation changes.

Although statistically significant, the correlations between Great Plains precipitation and tropical Pacific SSTs from the multi-century time series of the climate models never exceed 0.4-0.5. This means that no more than ~16-25% of the Great Plains precipitation variability can be accounted for by SST variations. Internal atmospheric variability and local feedbacks may be responsible for variations in precipitation not directly linked to SST variations. Schubert et al. (2004a) have also emphasized the large scatter among the ensemble members of their forced atmospheric simulations, indicating that the SST forcing is only part of the story. More recently, Hoerling et al. (2009) have examined the influence of SST on 20th century droughts in the Northern and Southern Plains separately, using both observations and a large ensemble of atmospheric simulations performed with three different atmospheric general circulation models. Their results support the conclusion that the causes for droughts in the two regions may be different, with the Southern Plains conditions being more likely influenced by SST forcing, primarily in the Pacific, and the Northern Plains droughts being mostly associated with internal atmospheric variability, thus presenting a lower degree of predictability. Further studies are needed to better quantify the influence of SST, and the degree of predictability of North American droughts at a more regional scale.

Acknowledgements

We acknowledge the international modeling groups for providing their data for analysis, the Program for Climate Model Diagnosis and Intercomparison (PCMDI) for collecting and archiving the model data, the JSC/CLIVAR Working Group on Coupled Modelling (WGCM) and their Coupled Model Intercomparison Project (CMIP) and Climate Simulation Panel for organizing the model data analysis activity, and the IPCC WG1 TSU for technical support. The IPCC Data Archive at Lawrence Livermore National Laboratory is supported by the Office of Science, US Department of Energy. Funding for AC was provided by NOAA through the U.S. CLIVAR Droughts in Coupled Models Project (DRICOMP), and through CDEP funding to ESRL. Insightful conversations with Clara Deser, as well as constructive criticism and suggestions from the NOAA/ESRL/PSD Attribution Group, in particular Martin Hoerling, Judith Perlwitz, Klaus Wolter, Dezheng Sun, are gratefully acknowledged.

References

- Alexander, M. A., J. Yin, G. Branstator, A. Capotondi, C. Cassou, R. Cullather, Y.-H. Kwon, J. Norris, J. Scott, and I. Wainer, 2006: Extratropical atmosphere-ocean variability in CCSM3. *J. Climate*, **19**, 2496-2525.
- Arblaster, J. M., G. A. Meehl, and A. Moore, 2002: Interdecadal modulation of Australian rainfall. *Climate Dyn.*, **18**, 519-531.
- Cook, E. R., C. Woodhouse, C. M. Eakin, D. M. Meko, and D. W. Stahle, 2004: Long term aridity changes in the western United States. *Science*, **306**, 1015-1018.
- Douglass, A. E., 1929: The secrets of the southwest solved by talkative tree rings. *National Geographic*, **54**, 737-770.
- Douglass, A. E., 1935: Dating Pueblo Bonito and other ruins of the southwest. Technical Report Pueblo Bonito series No. 1, National Geographic Society, Washington, DC, 74 pp.

- Herweijer, C., R. Seager, and E. R. Cook, 2007: North American droughts of the last millennium from a gridded network of tree ring data. *J. Climate*, **20**, 1353-1379.
- Hoerling, M. P., and A. Kumar, 2003: The perfect ocean for drought. *Science*, **299**, 691-694.
- Hoerling, M. P., X.-W. Quan, and J. Eischeid, 2009: Distinct causes for two principal U.S. droughts of the 20th Century, *Geophys. Res. Lett.*, in review.
- Kwon, Y.-H., and C. Deser, 2007: North Pacific decadal variability in the Community Climate System Model version 2. *J. Climate*, **20**, 2416-2433.
- Liang, X.-Z., J. Zhu, K. E. Kunkel, M. Ting, and J. X. L. Wang, 2008: Do CGCMs simulate the North American Monsoon precipitation seasonal-interannual variability? *J. Climate*, **21**, 4424-4448.
- Lu, J., G. Chen, and D. M. W. Frierson, 2008: Response of the zonal mean atmospheric circulation to El Niño versus global warming. *J. Climate*, **21**, 5835-5851.
- Mantua, N. J., S. R. Hare, Y. Zhang, J. M. Wallace, and R. C. Francis, 1997: A Pacific interdecadal oscillation with impacts on salmon production. *Bull. Amer. Meteor. Soc.*, **78**, 1069-1079.
- McAfee, S. A., and J. L. Russell, 2009: Attenuated orography contributes to precipitation errors over the western United States in Intergovernmental Panel on Climate Change Fourth Assessment Report models. *J. Climate*, submitted.
- Meehl, G. A., and A. Hu, 2006: Megadroughts in the Indian monsoon region and southwest North America and a mechanism for associated multidecadal Pacific sea surface temperature anomalies. *J. Climate*, **19**, 1605-1623.
- Power, S., T. Casey, C. Folland, A. Colman, and V. Metha, 1999: Interdecadal modulation of the impact of ENSO on Australia. *Climate Dyn.* **15**, 319-324.
- Schubert, S. D., M. J. Suarez, P. J. Pegion, R. D. Koster, and J. T. Bacmeister, 2004a: Causes of long-term drought in the United States Great Plains. *J. Climate*, **17**, 485-503.
- Schubert, S. D., M. J. Suarez, P. J. Pegion, R. D. Koster, and J. T. Bacmeister, 2004b: On the cause of the 1930s Dust Bowl. *Science*, **303**, 1855-1859.

- Seager, R., Y. Kushnir, C. Herweijer, N. Naik, and J. Velez, 2005: Modeling of tropical forcing of persistent droughts and pluvials over western North America: 1856-2000. *J. Climate*, **18**, 4065-4088.
- Seager, R., N. Graham, C. Herweijer, A. L. Gordon, Y. Kushnir, and E. Cook, 2007: Blueprints for Medieval hydroclimate. *Quaternary Science Reviews*, doi:10.1016/j.quascirev.2007.04.020.
- Seager, R., Y. Kushnir, M. Ting, M. Cane, N. Naik, and J. Miller, 2008: Would advance knowledge of 1930s SSTs have allowed prediction of the Dust Bowl drought? *J. Climate*, **21**, 3261-3281.
- Smith, T. M., R. W. Reynolds, T. C. Peterson, and J. Lawrimore, 2008: Improvements to NOAA's historical merged land-ocean surface temperature analysis (1880-2006). *J. Climate*, **21**, 2283-2296.
- Stine, S., 1994: Extreme and persistent drought in California and Patagonia during medieval time. *Nature*, **369**, 546-549.
- Ting, M., and H. Wang, 1997: Summertime U.S. precipitation variability and its relation to Pacific Sea Surface Temperature. *J. Climate*, **10**, 1853-1873.
- Trenberth, K. E., 1984: Some effects of finite sample size and persistence on meteorological statistics. Part I: Autocorrelations. *Mon. Wea. Rev.*, **112**, 2359-2368.

Figure captions

Figure 1. Annual mean precipitation over North America (mm/day) from the GPCC data set. Contour interval is 0.5 mm/day. Values larger than 1 mm/day are shaded.

Figure 2. Same as Figure 1, but for the six climate models. Annual averages are based upon the total duration of the picntrl simulations.

Figure 3. Seasonal cycle of precipitation in the GP region from the GPCC data set (black line), and the six climate models.

Figure 4. a) Evolution of precipitation over the GP region from the GPCC data set. The thin curve is based on annual values, while the thick curve is obtained by applying a 5-year running mean to the annual values. The standard deviation of the 5-year running mean time series is 0.11 mm/day. b) Monthly standard deviation of the 5-year running mean precipitation.

Figure 5. Low-pass filtered time series of GP precipitation for the six climate models over the duration of their PICNTRL simulations. The low-pass filtering has been performed by applying a 5-year running mean to the annual values. The standard deviations of the time series is shown in the right bottom corner of each panel. The red segments in a) indicate the periods considered for composites.

Figure 6. Standard deviation of 5-year running mean precipitation as a function of calendar month for the six climate models. The dot-dash line shows the monthly standard deviation of precipitation for GPCC.

Figure 7. Composites of SST (red–blue shading over the ocean) and precipitation (orange-green shading) over land for the GFDL_CM2.1 model, over the years 38-55 (top-left), 170-175 (top-right), and 240-254 (bottom-left). All the periods considered are characterized by lower-than-average 5-year running mean precipitation in the GP region.

The bottom-right panel shows the average of the three composites. SST contour interval is 0.2°C , with values larger (in absolute value) than 0.2 shaded. Precipitation contour interval is 0.1 mm/day. Values larger than 0.05 are shaded.

Figure 8. a) Time series of precipitation in the GP region during the first 100 years of the simulation. This line indicates the yearly values, while the thick line shows the low-pass filtered curve. b) Same as in a), but for the period 160-260. c) Evolution of SST in the box $140^{\circ}\text{E}-180^{\circ}\text{E}$, $5^{\circ}\text{S}-5^{\circ}\text{N}$, based on annual values for the period 1-100. d) Same as in c), but for the period 160-260. e) Evolution of SST in the box $150^{\circ}\text{W}-110^{\circ}\text{W}$, $5^{\circ}\text{S}-5^{\circ}\text{N}$, based on annual values over the period 1-100. f) Same as in e), but for the period 160-260. The thicker line in panels c)-f) highlights the periods considered for the composites.

Figure 9. Correlation between 5-year running mean GPCP precipitation and 5-year running mean NOAA.ERSST. Orange shading is for positive values, and blue shading is for negative values. Contour interval is 0.1. Values larger than 0.45, and lower than -0.45 are shaded, with orange shading for positive values, and blue shading for negative values. Correlations larger, in absolute values, than 0.45 are statistically significant at the 95% level.

Figure 10. Correlation between the 5-year running mean of GP precipitation and 5-year running mean of SST for the six climate models. Values larger than 0.2 in absolute value are shaded. Orange shading is for positive values, while blue shading is for negative values. Correlations larger than 0.2 are statistically significant at the 95% level for GFDL_CM2.1, GFDL_CM2.0, and CCSM3, while for the HadCM3, CSIRO, and CCCMA the threshold for statistical significance at the 95% level is 0.25. The Great Plains area is shown by the box over North America.

Figure 11. Correlations between 5-year running mean GP precipitation and 5-year running mean global precipitation for the six climate models. Values larger than 0.1 in absolute value are shaded, and values larger than 0.2 in absolute value are also contoured. Contour interval is 0.1. Correlations larger than 0.2 are statistically significant at the 95%

level. Green shading is for positive values (larger than average precipitation), while brown shading is for negative values (lower than average precipitation).

Figure 12. Correlations between the 5-yrs running mean GP precipitation and 5-yrs running mean 200mb geopotential height for the six climate models. Values larger than 0.1 in absolute value are shaded, and values larger than 0.2 in absolute value are also contoured. Contour interval is 0.1. Correlations larger than 0.2 are statistically significant at the 95% level. Orange shading is for positive height anomalies, while blue shading is for negative height anomalies.

Figure 13. Correlations between the 5-yrs running mean GP precipitation and 5-yrs running mean zonal mean zonal wind (shading) for the six climate models, superimposed upon the mean zonal mean zonal wind (contours, C.I. 5m/s). Orange shading is for positive values, while blue shading is for negative values. Correlations larger than ~ 0.2 in absolute value are statistically significant at the 95% level. The negative correlations at the poleward flanks of the mean jet and the positive correlations at the equatorward flanks of the jets are an indication of an equatorward displacement of the jets in both hemispheres during periods of larger than average precipitation in the Great Plains.

Figure 14. Top panel shows the leading EOF of 5-year running mean SST from the NOAA.ERSST data set. Contour interval is 1°C . Values whose magnitude is larger than 0.5 are shaded. Orange shading is for positive values, and blue shading is for negative values. The EOF accounts for 30% of the low-frequency SST variance. Bottom panel shows the comparison between the Principal Component of the leading SST EOF (solid line) and the 5-year running mean precipitation from GPCC (dot-dash line). Correlation coefficient between the two time series is 0.56, statistically significant at the 95% level.

Figure 15. Leading EOF for the six climate models. Contour interval is 1°C . Values whose magnitude is larger than 0.5 are shaded. Orange shading is for positive values, and blue shading is for negative values. The fraction of variance explained is 29% for

GFDL_CM2.1, 26% for GFDL_CM2.0, 28% for CCSM3, 26% for HadCM3, 20% for CSIRO, and 27% for CCCMA.

Figure 16. The evolution of the PC of the leading decadal SST mode in the Pacific Ocean (solid line) for all the six climate models is compared with the decadal evolution of GP precipitation (dot-dash line). Precipitation units are mm/day. The correlation coefficient between the two time series is shown in each panel. The numbers in parentheses indicate the correlations corresponding to the 95% significant level for each model.

<i>Model</i>	<i>Country</i>	<i>Ocean Resolution</i>	<i>Atmospheric Resolution</i>	<i>Duration (yrs)</i>
GFDL_CM2.1	USA	1° x 0.33°L50	2.5° x 2° L24	500
GFDL_CM2.0	USA	1° x 0.33°L50	2.5° x 2° L24	500
NCAR_CCSM3	USA	1.125° x 0.27°L40	T85L26	500
UKMO_HadCM3	UK	1.25° x 1.25° L20	3.75° x 2.5° L19	341
CSIRO_Mk3.0	Australia	1.875° x 0.84° L31	T63L18	380
CCCMA	Canada	1.4° x 0.94° L29	T63L31	350

Table 1. Information about the six climate models used in this study, including country where the model was developed, resolution of the ocean and atmospheric components (lon, lat, vertical), and duration of the pre-industrial control simulations.

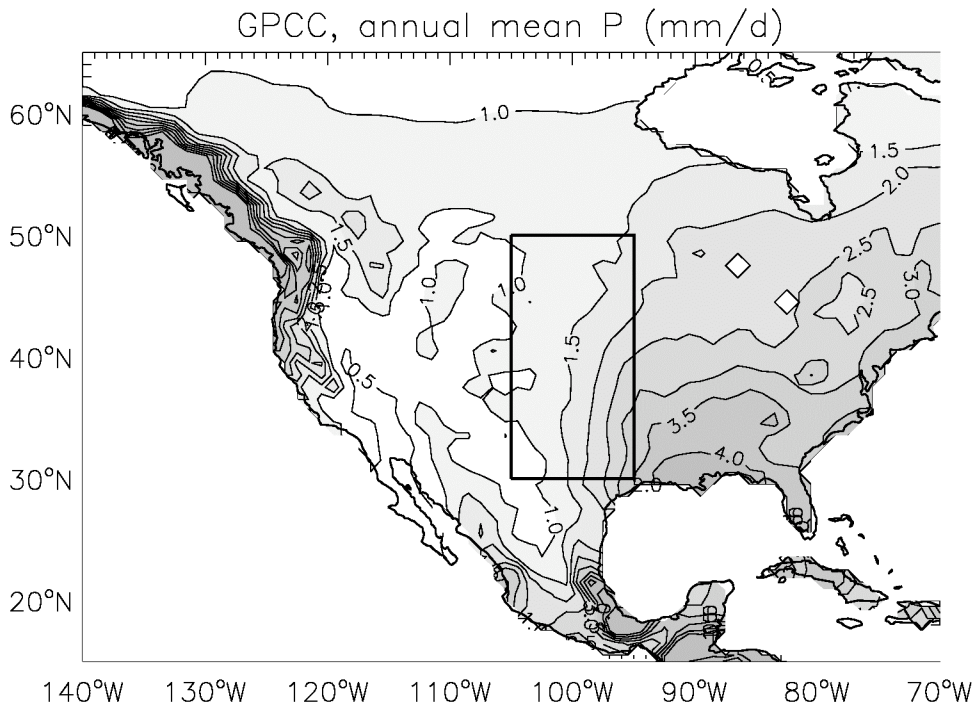


Figure 1. Annual mean precipitation over North America (mm/day) from the GPCC data set. Contour interval is 0.5 mm/day. Values larger than 1 mm/day are shaded.

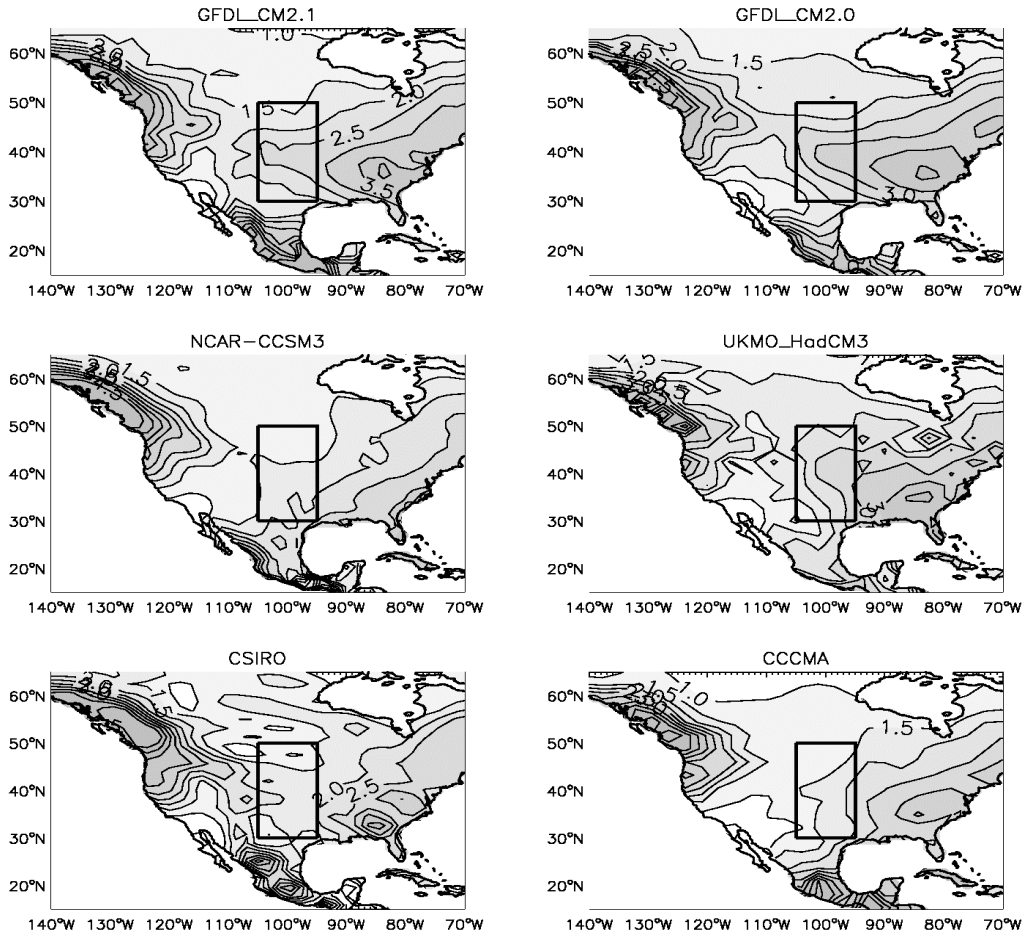


Figure 2. Same as Figure 1, but for the six climate models. Annual averages are based upon the total duration of the picntrl simulations.

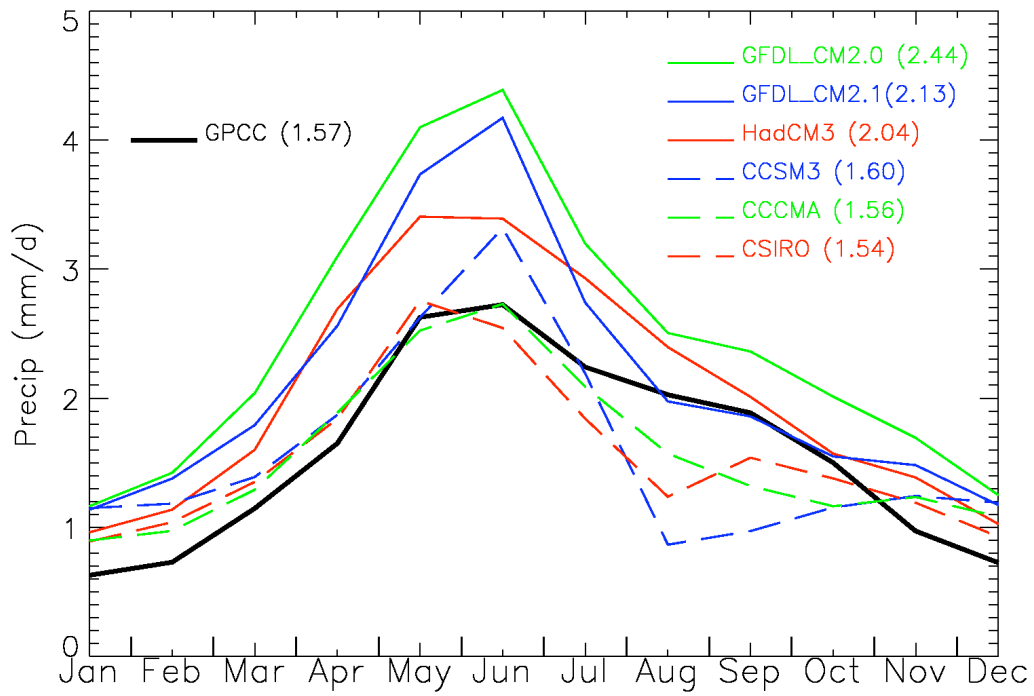


Figure 3. Seasonal cycle of precipitation in the GP region from the GPCP data set (black line), and the six climate models.

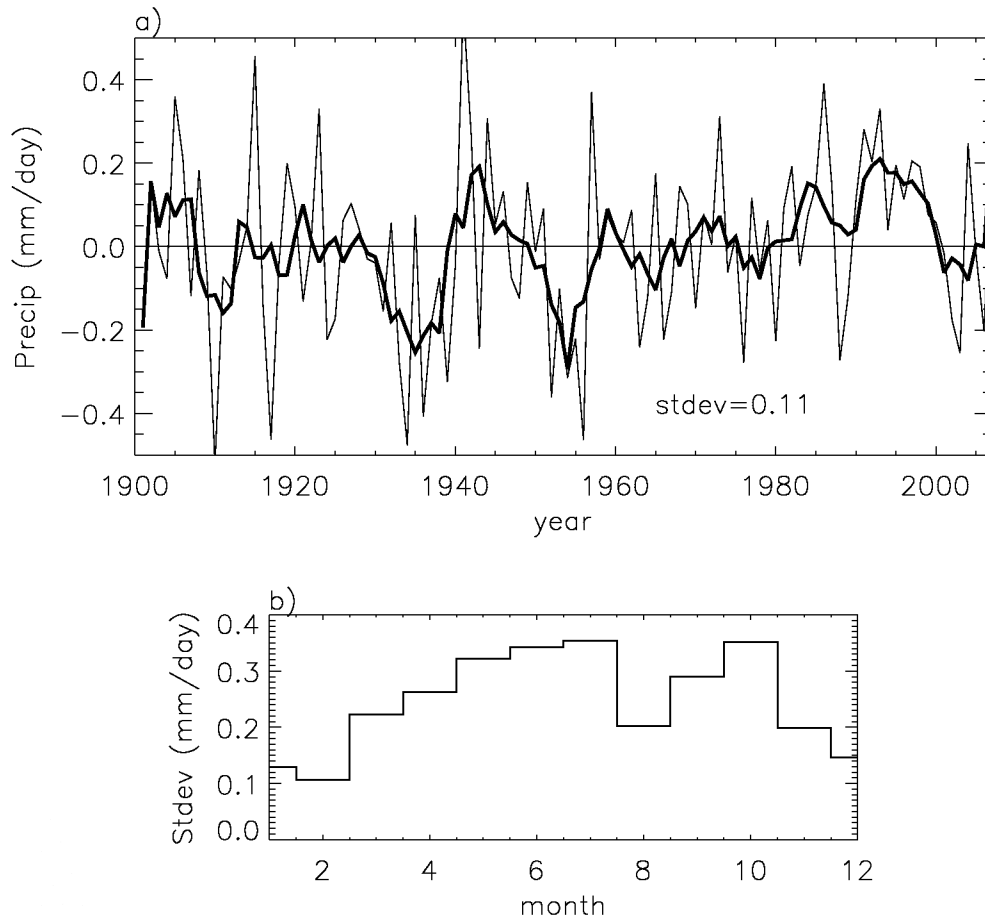


Figure 4. a) Evolution of precipitation over the GP region from the GPCP data set. The thin curve is based on annual values, while the thick curve is obtained by applying a 5-year running mean to the annual values. The standard deviation of the 5-year running mean time series is 0.11 mm/day. b) Monthly standard deviation of the 5-year running mean precipitation.

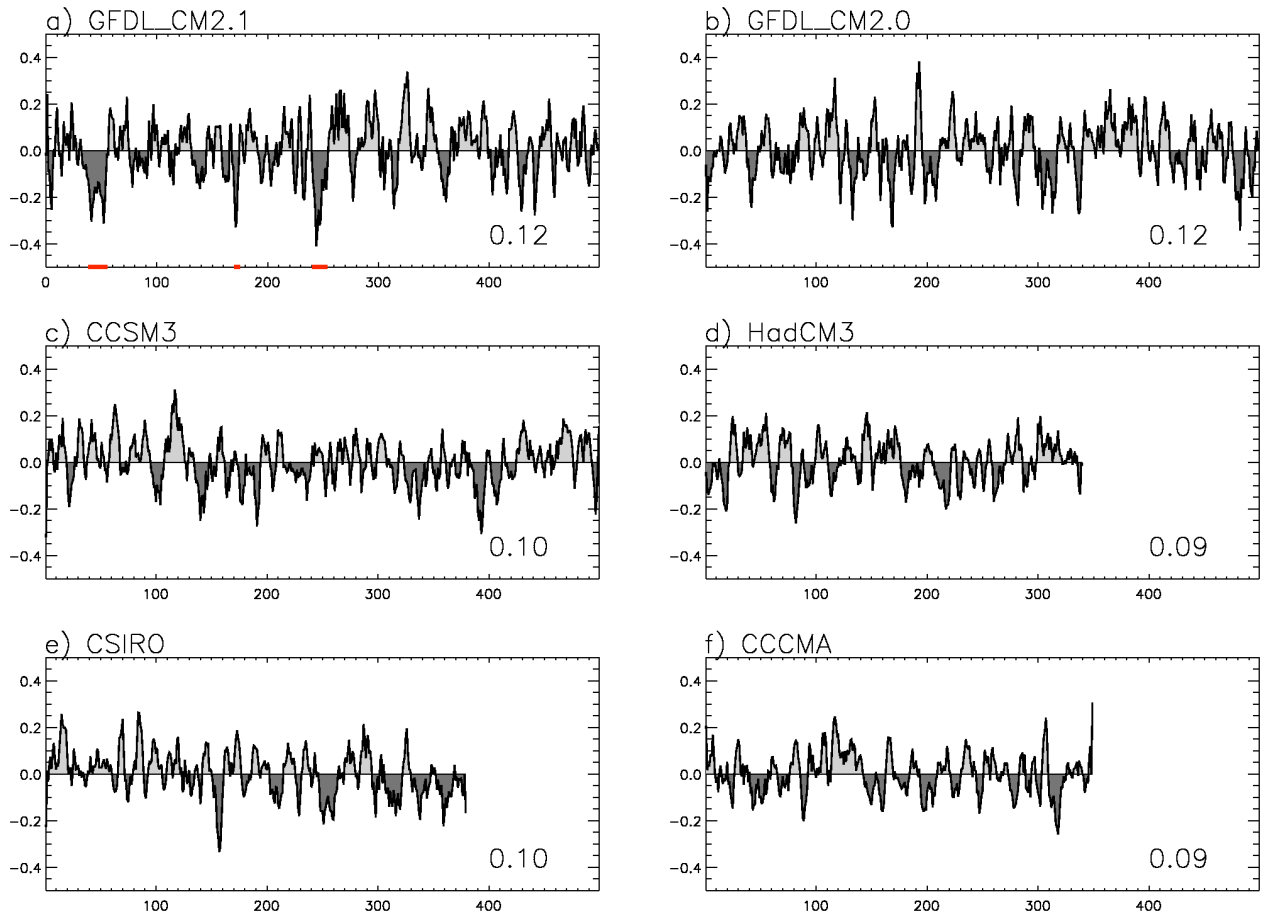


Figure 5. Low-pass filtered time series of GP precipitation for the six climate models over the duration of their PICNTRL simulations. The low-pass filtering has been performed by applying a 5-year running mean to the annual values. The standard deviations of the time series is shown in the right bottom corner of each panel. The red segments in a) indicate the periods considered for composites.

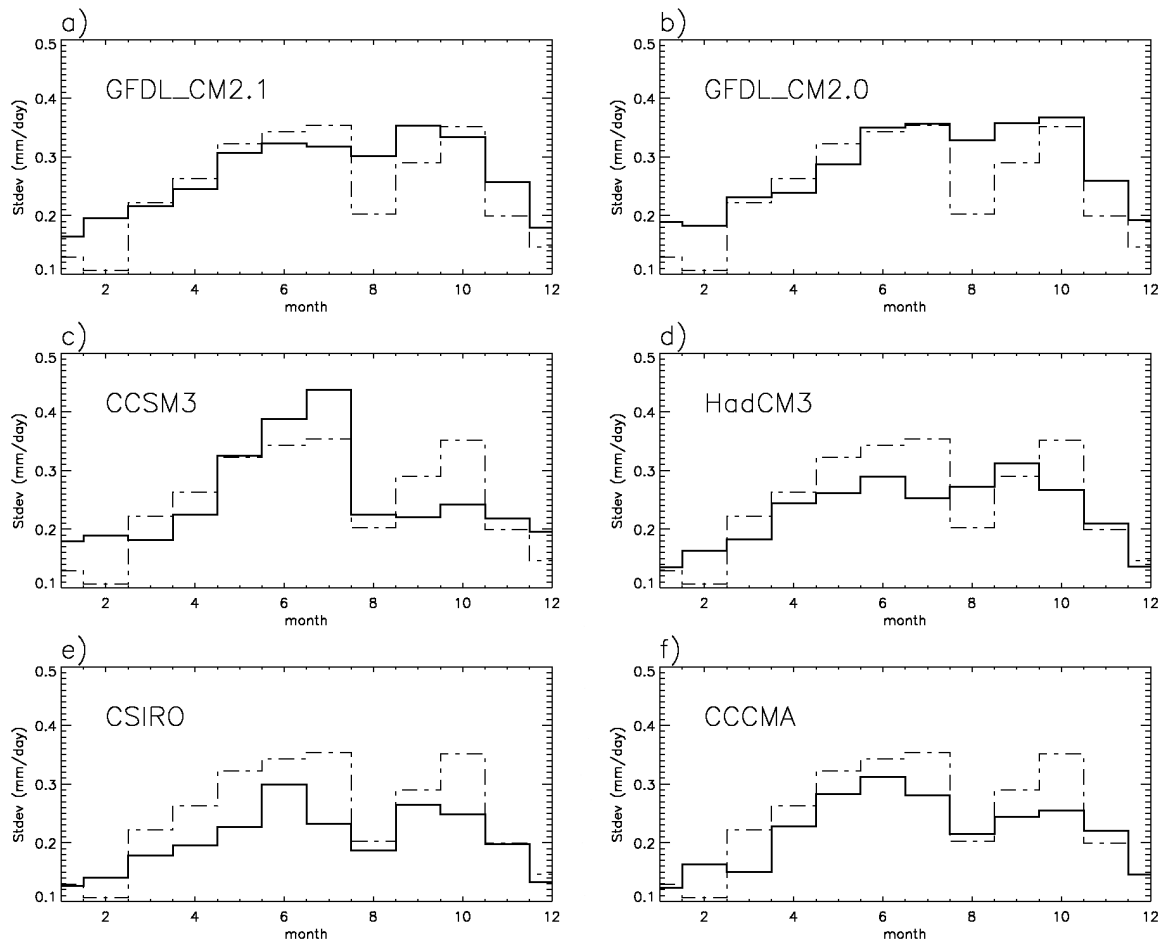


Figure 6. Standard deviation of 5-year running mean precipitation as a function of calendar month for the six climate models. The dot-dash line shows the monthly standard deviation of precipitation for GPCC.

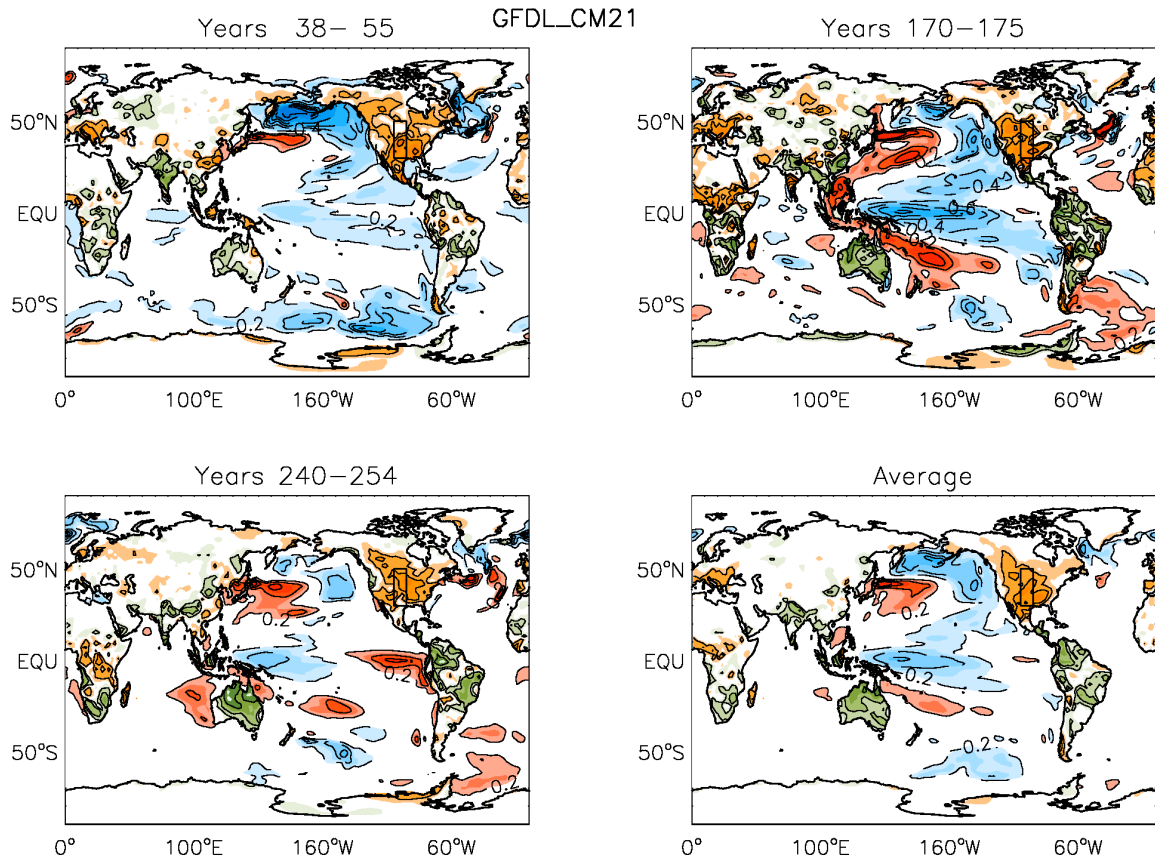


Figure 7. Composites of SST (red –blue shading over the ocean) and precipitation (orange-green shading) over land for the GFDL_CM2.1 model, over the years 38-55 (top-left), 170-175 (top-right), and 240-254 (bottom-left). All the periods considered are characterized by lower-than-average 5-year running mean precipitation in the GP region. The bottom-right panel shows the average of the three composites. SST contour interval is 0.2°C , with values larger (in absolute value) than 0.2 shaded. Precipitation contour interval is 0.1 mm/day . Values larger than 0.05 are shaded.

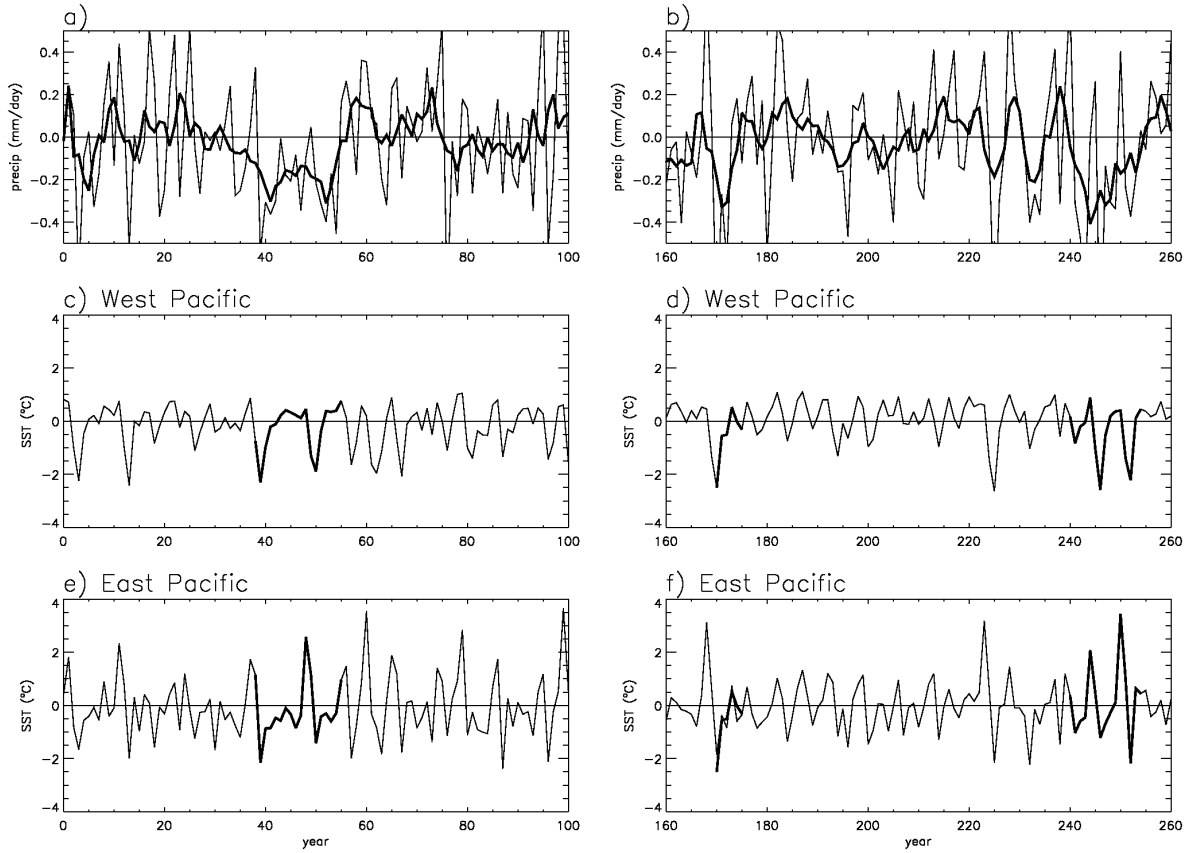


Figure 8. a) Time series of precipitation in the GP region during the first 100 years of the simulation. This line indicates the yearly values, while the thick line shows the low-pass filtered curve. b) Same as in a), but for the period 160-260. c) Evolution of SST in the box 140°E-180°E, 5°S-5°N, based on annual values for the period 1-100. d) Same as in c), but for the period 160-260. e) Evolution of SST in the box 150°W-110°W, 5°S-5°N, based on annual values over the period 1-100. f) Same as in e), but for the period 160-260. The thicker line in panels c)-f) highlights the periods considered for the composites.

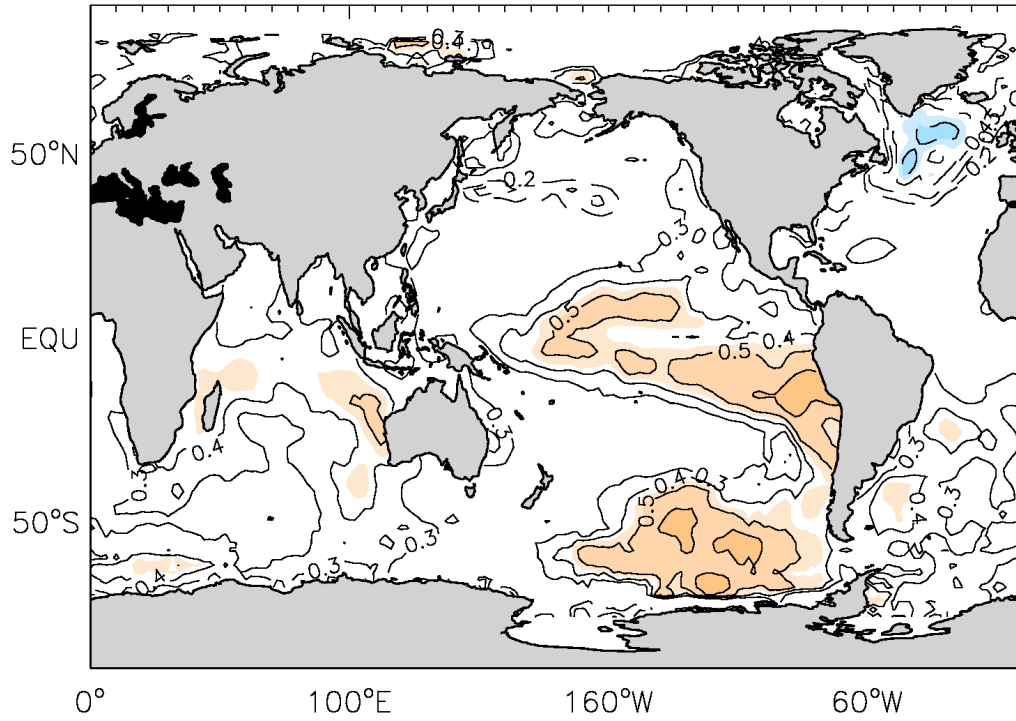


Figure 9. Correlation between 5-year running mean GPCP precipitation and 5-year running mean NOAA.ERSST. Orange shading is for positive values, and blue shading is for negative values. Contour interval is 0.1. Values larger than 0.45, and lower than -0.45 are shaded, with orange shading for positive values, and blue shading for negative values. Correlations larger, in absolute values, than 0.45 are statistically significant at the 95% level.

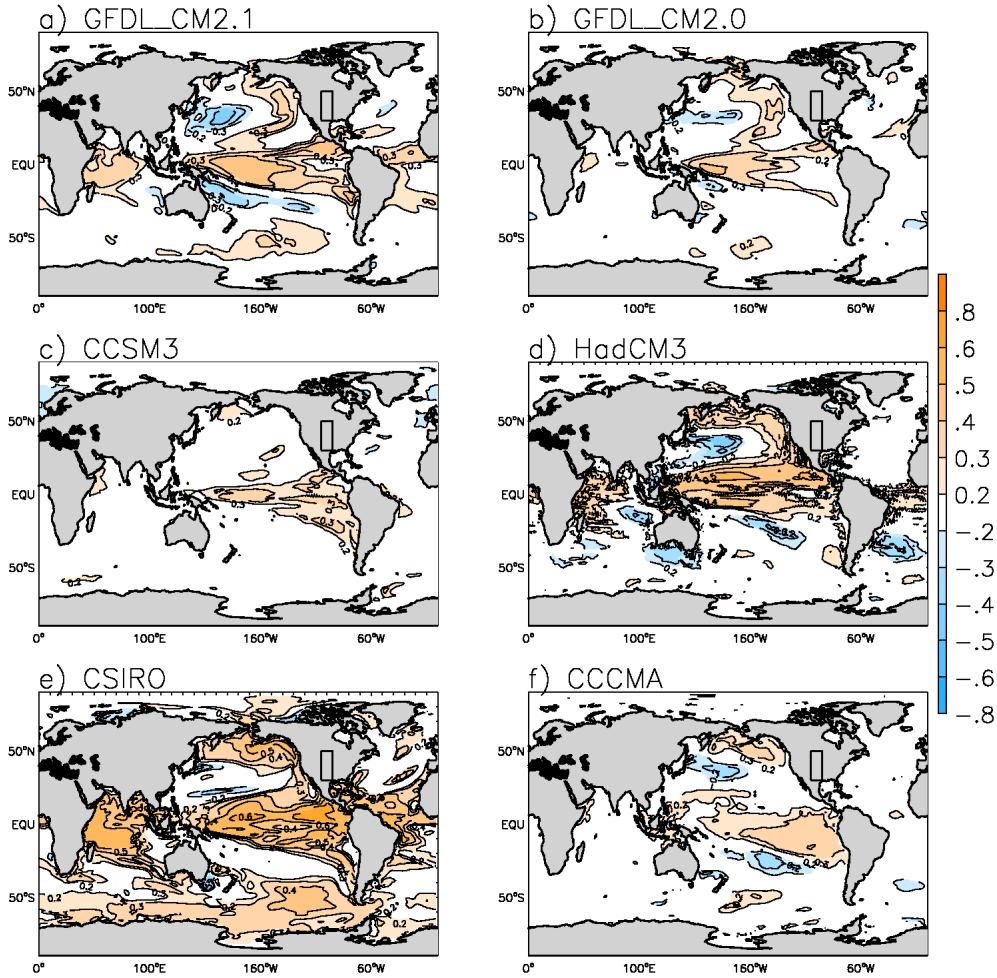


Figure 10. Correlation between the 5-year running mean of GP precipitation and 5-year running mean of SST for the six climate models. Values larger than 0.2 in absolute value are shaded. Orange shading is for positive values, while blue shading is for negative values. Correlations larger than 0.2 are statistically significant at the 95% level for GFDL_CM2.1, GFDL_CM2.0, and CCSM3, while for the HadCM3, CSIRO, and CCCMA the threshold for statistical significance at the 95% level is 0.25. The Great Plains area is shown by the box over North America.

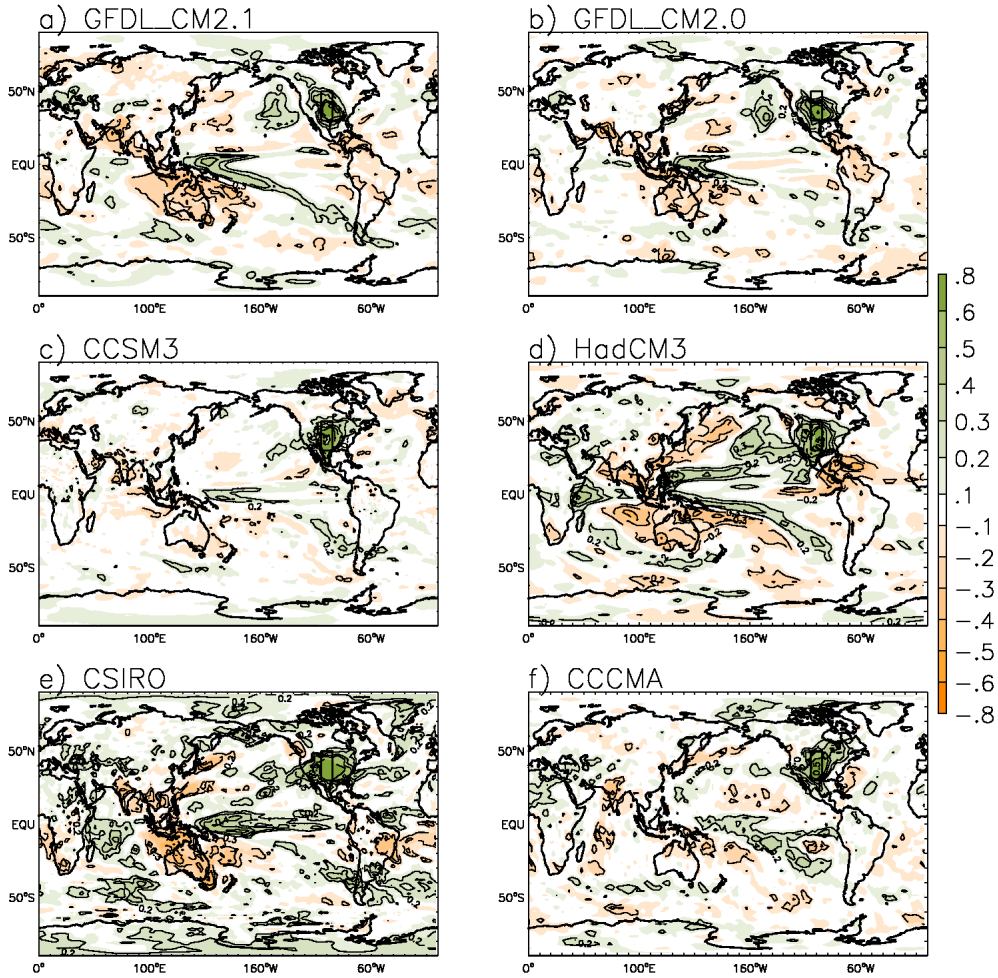


Figure 11. Correlations between 5-year running mean GP precipitation and 5-year running mean global precipitation for the six climate models. Values larger than 0.1 in absolute value are shaded, and values larger than 0.2 in absolute value are also contoured. Contour interval is 0.1. Correlations larger than 0.2 are statistically significant at the 95% level. Green shading is for positive values (larger than average precipitation), while brown shading is for negative values (lower than average precipitation).

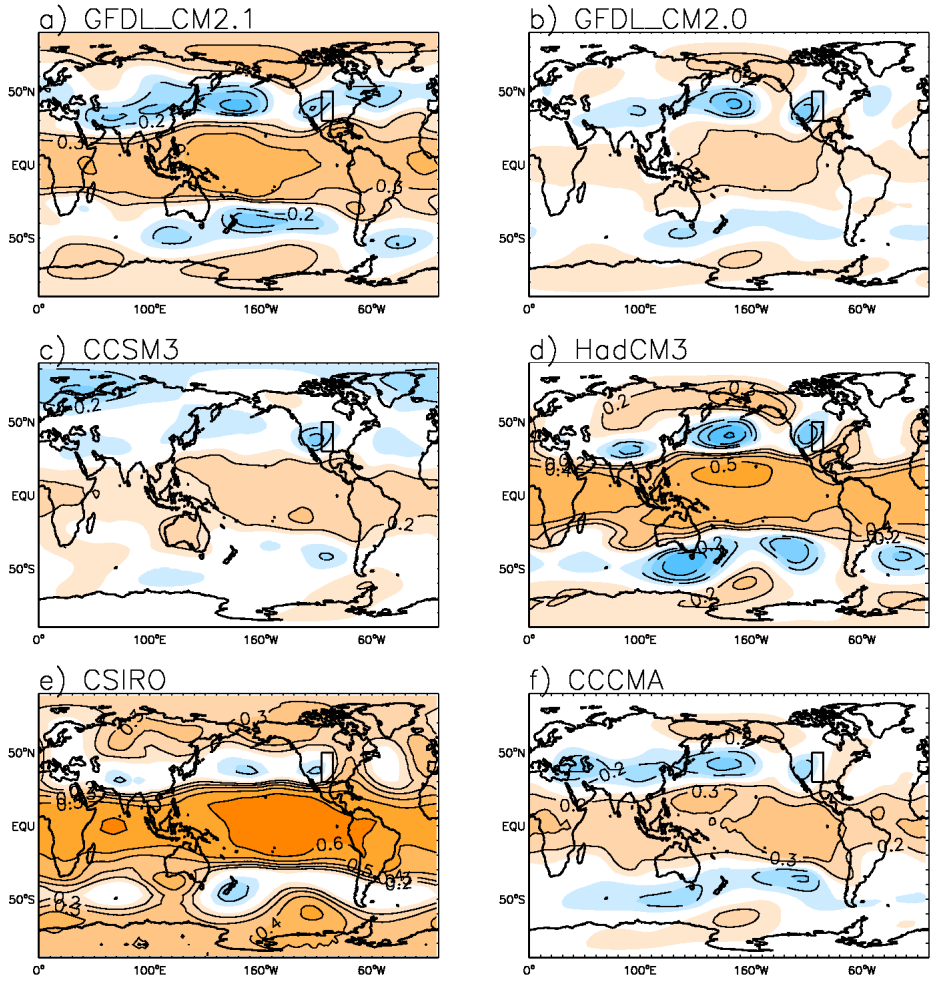


Figure 12. Correlations between the 5-yr running mean GP precipitation and 5-yr running mean 200mb geopotential height for the six climate models. Values larger than 0.1 in absolute value are shaded, and values larger than 0.2 in absolute value are also contoured. Contour interval is 0.1. Correlations larger than 0.2 are statistically significant at the 95% level. Orange shading is for positive height anomalies, while blue shading is for negative height anomalies.

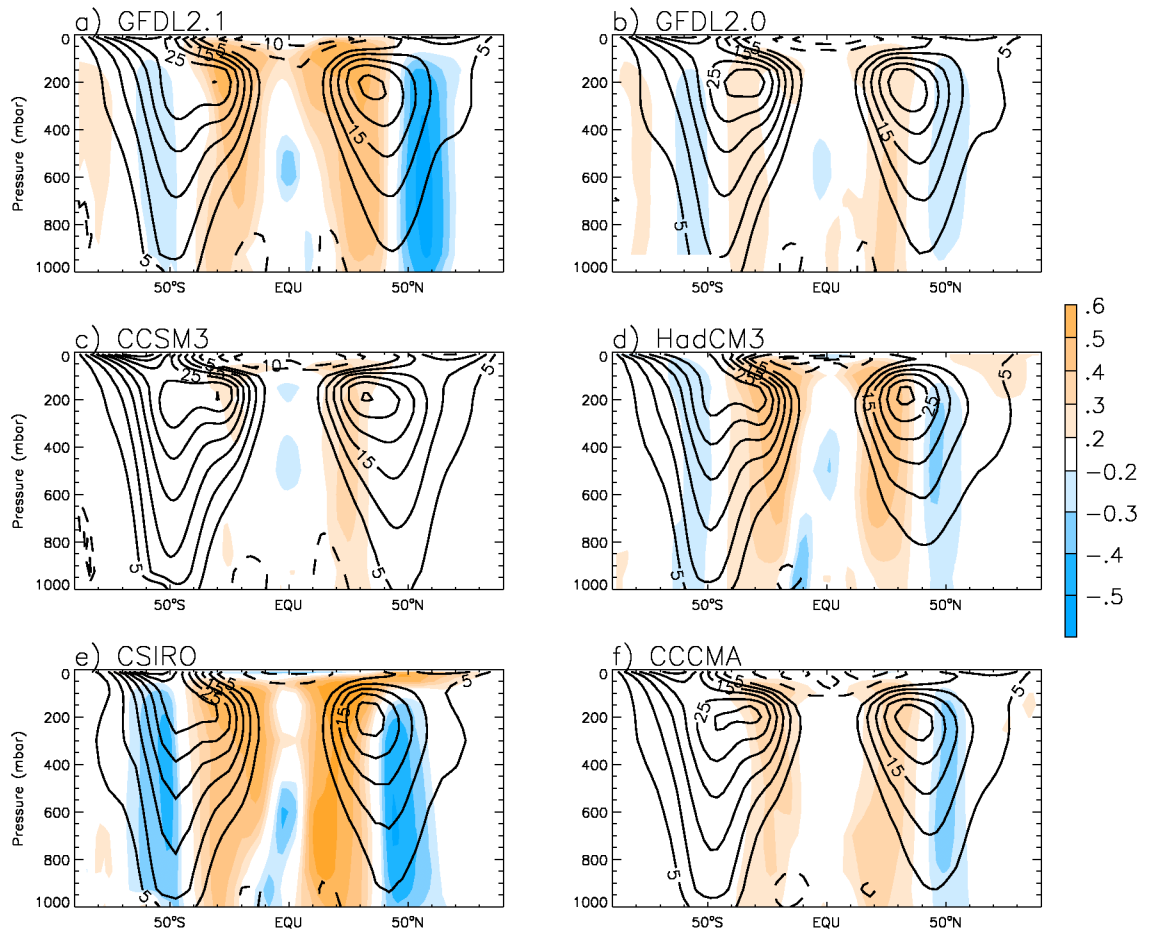


Figure 13. Correlations between the 5-yr running mean GP precipitation and 5-yr running mean zonal mean zonal wind (shading) for the six climate models, superimposed upon the mean zonal mean zonal wind (contours, C.I. 5m/s). Orange shading is for positive values, while blue shading is for negative values. Correlations larger than ~ 0.2 in absolute value are statistically significant at the 95% level. The negative correlations at the poleward flanks of the mean jet and the positive correlations at the equatorward flanks of the jets are an indication of an equatorward displacement of the jets in both hemispheres during periods of larger than average precipitation in the Great Plains.

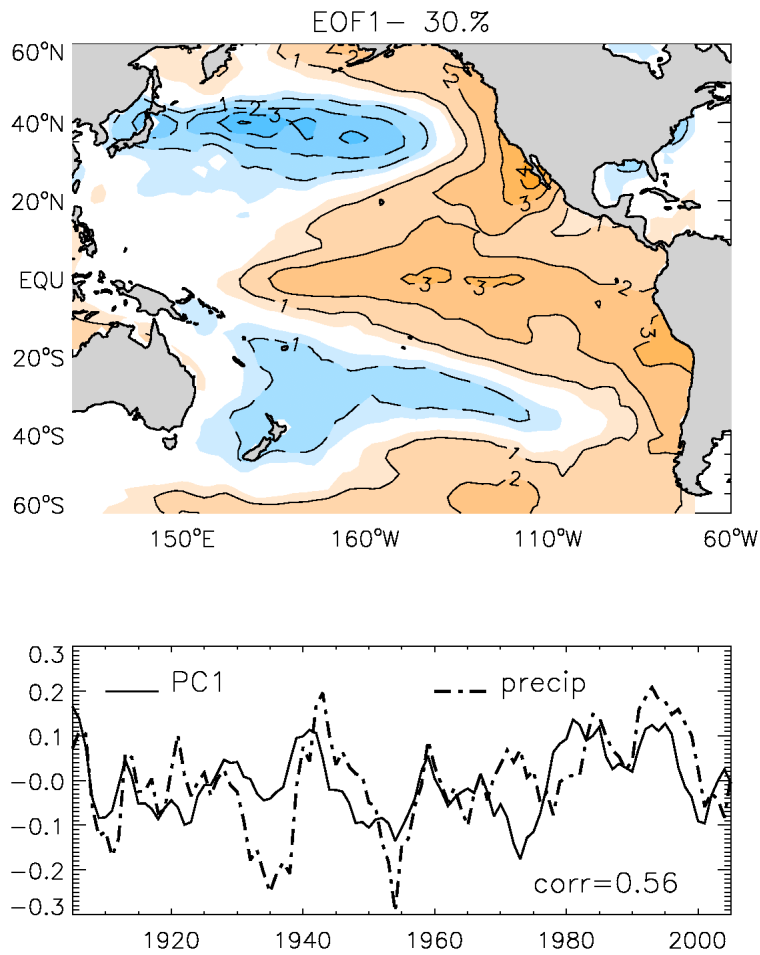


Figure 14. Top panel shows the leading EOF of 5-year running mean SST from the NOAA.ERSST data set. Contour interval is 1°C. Values whose magnitude is larger than 0.5 are shaded. Orange shading is for positive values, and blue shading is for negative values. The EOF accounts for 30% of the low-frequency SST variance. Bottom panel shows the comparison between the Principal Component of the leading SST EOF (solid line) and the 5-year running mean precipitation from GPCC (dot-dash line). Correlation coefficient between the two time series is 0.56, statistically significant at the 95% level.

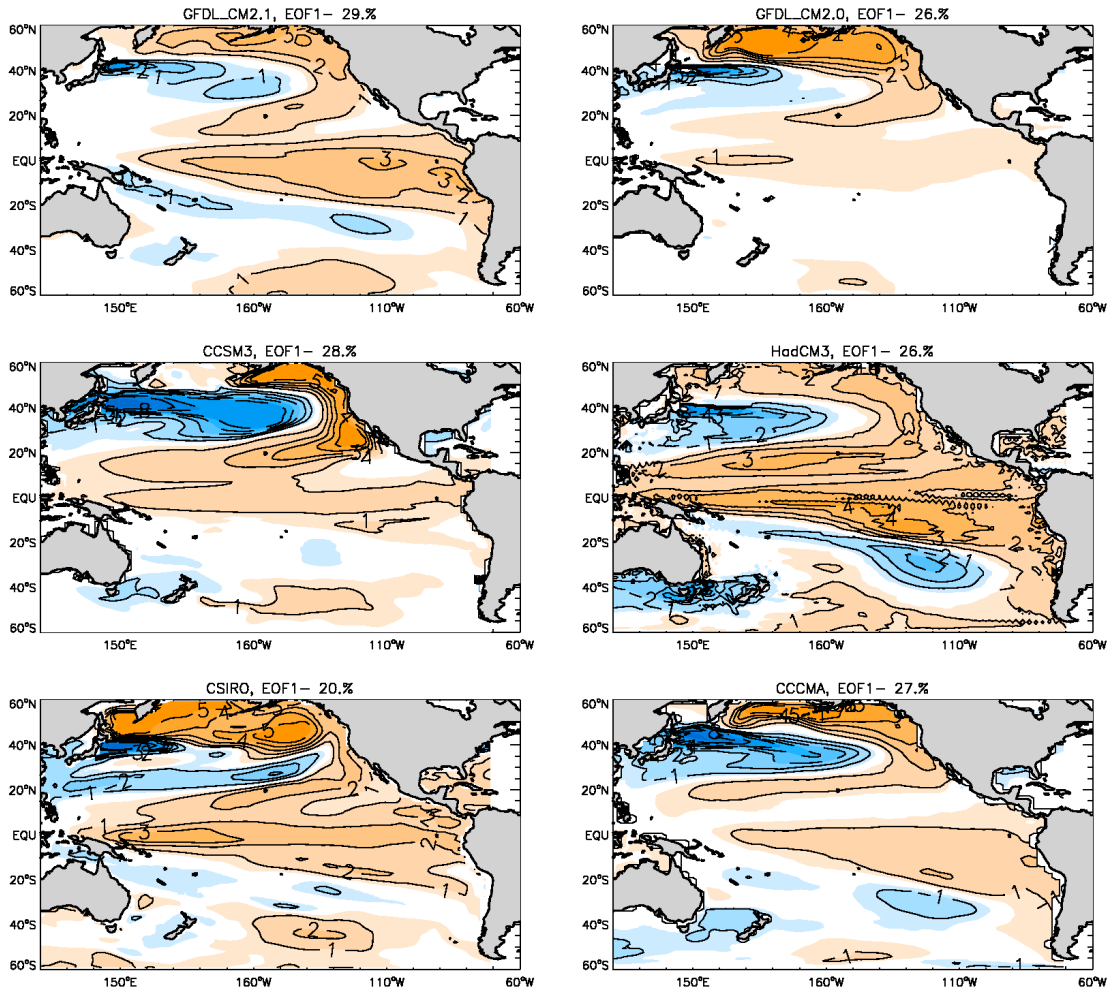


Figure 15. Leading EOF for the six climate models. Contour interval is 1°C. Values whose magnitude is larger than 0.5 are shaded. Orange shading is for positive values, and blue shading is for negative values. The fraction of variance explained is 29% for GFDL_CM2.1, 26% for GFDL_CM2.0, 28% for CCSM3, 26% for HadCM3, 20% for CSIRO, and 27% for CCCMA.

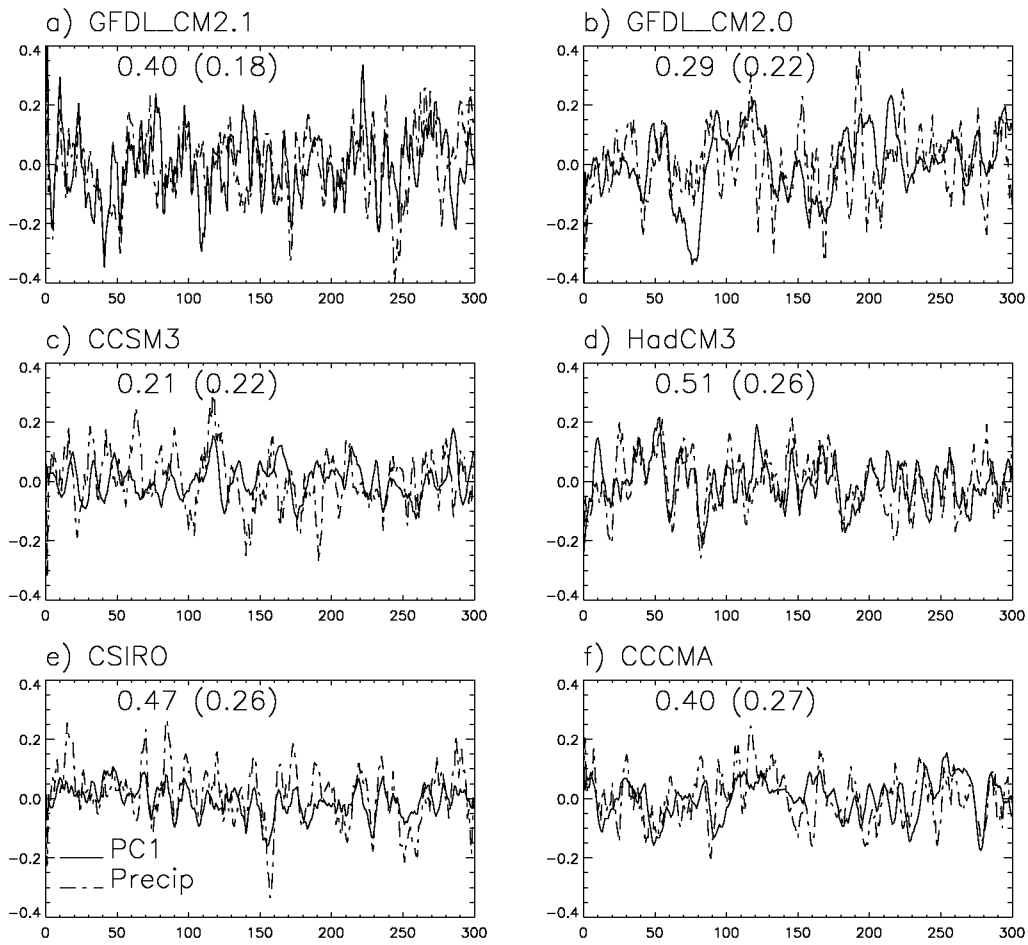


Figure 16. The evolution of the PC of the leading decadal SST mode in the Pacific Ocean (solid line) for all the six climate models is compared with the decadal evolution of GP precipitation (dot-dash line). Precipitation units are mm/day. The correlation coefficient between the two time series is shown in each panel. The numbers in parentheses indicate the correlations corresponding to the 95% significant level for each model.

